buildings

Article

Nonlinear Behavior of Bonded and Unbonded Two-Way Post-Tensioned Slabs Pre-Strengthened with CFRP Laminates

Mohammed M. Attia [1,*], Ayman H. H. Khalil [2], Ghada N. Mohamed [3], Morcos F. Samaan [3] and Dušan Katunský [4]

[1] Civil and Architectural Constructions Department, Faculty of Technology and Education, Suez University, Suez 43511, Egypt
[2] Civil Engineering Department, Ain Shams Faculty of Engineering, Ain Shams University, Cairo 1175, Egypt
[3] Civil Engineering Department, The High Technological Institute, 10th of Ramadan City 44629, Egypt
[4] Institute of Architectural Engineering, Faculty of Civil Engineering, Technical University of Košice, 04001 Košice, Slovakia
* Correspondence: mohammed.mahmoudattia@suezuni.edu.eg

Abstract: In this study, hybrid nonlinear finite element models (FEM) were developed to examine the flexural performance and the ultimate load capacity of bonded and unbonded two-way reinforced concrete post-tensioned (PT) slabs that were pre-strengthened with external carbon-fiber reinforcement polymer (CFRP) laminates. Full 3D simulations, using ANSYS models, have been created for five different slab samples that were selected from a previously available experimental study. The model results were assessed to enable further numerical analysis. The result calibration included measurements of first crack loads, ultimate loads, deflections, strains in the extreme fiber of concrete, strains in CFRP laminates, and failure modes. The results proved a good correlation between FEM output and experimental ones. Based on this, the influencing parameters that affect plate stiffness, as well as the bending capacity of PT slabs, were examined by performing a detailed parametric study. The parameters included real-life load simulation, cable-to-CFRP strength contribution, and CFRP laminate location selection. The results demonstrated that strengthening using CFRP laminates have significantly increased the ductility index of both bonded and unbonded PT concrete slabs by 62.18% and 59.87%, respectively. In addition, strip strengthening locations near supports are much more effective than in the middle of slabs. Additionally, the CFRP strengthening contribution is very considerable in slabs with low PT ratios.

Keywords: post-tension; concrete slab; finite elements; ANSYS; CFRP laminates; flexural performance; failure patterns; pre-strengthening

Citation: Attia, M.M.; Khalil, A.H.H.; Mohamed, G.N.; Samaan, M.F.; Katunský, D. Nonlinear Behavior of Bonded and Unbonded Two-Way Post-Tensioned Slabs Pre-Strengthened with CFRP Laminates. *Buildings* **2023**, *13*, 35. https://doi.org/10.3390/buildings13010035

Academic Editor: Elena Ferretti

Received: 15 October 2022
Revised: 14 December 2022
Accepted: 20 December 2022
Published: 23 December 2022

1. Introduction

Prestressed concrete has been rapidly used in numerous fields of structural engineering, because of the enormous development in building techniques and the increasing need for long-span members [1]. Pre-tensioned and post-tensioned concrete are two types of prestressed concrete, while the post-tension technic has several advantages [2]. In pre-tension, the cables are tensioned between two fixed supports then the concrete is cast around the cables, which are cut from the supports once the concrete has reached its strength [3,4]. Post-tensioned concrete is used with the formwork in the site, the concrete is cast around corrugated ducts, which are fixed to any required profile [5,6]. The cables are usually unstressed in the ducts during the concrete casting. When the concrete has reached its strength, the cables are tensioned. The concrete is compressed during the stressing operation and the prestress is kept after the cables are anchored by bearing the end anchorage plates onto the concrete [7,8]. After the cables have been anchored, the corrugated ducts including the cables are often filled with grout. In this method, the cables are bonded to the concrete and are more efficient in controlling cracks and providing ultimate strength [9]. In some situations, cables are not grouted for reasons of economy and remain permanently unbonded [10]. However, prestressing can be divided into fully prestressing, which focused on the complete removal of tensile stresses in members at normal service loads [10], and partial prestressing, which is a medium solution between fully prestressed concrete and ordinary RC [11]. One of the problems that have faced PT applications is that the fully prestressed concrete members experienced low ductility [10,12,13].

On the other hand, because of changes in laws and provisions, as well as changes in the use of buildings, it is highly recommended that old structures be rehabilitated and strengthened [14,15]. In the last years of the previous century, real progress in research took place using fiber-reinforced polymers (FRPs) in strengthening applications [16–18]. FRPs are considered a better alternative than steel plates because of their multiple characteristics such as high tensile capacity, non-corrosive nature, and lightweight [19–21]. The method of manufacturing pre-cured laminate is about the impregnation of fibers with adhesive, which is then pultruded and cured by the manufacturer. The most important result in manufacturing the pre-cured laminate can create laminates that are stronger and stiffer per unit volume than equivalent wet lay-up laminates [22]. Typically, laminates used for concrete strengthening are unidirectional and have all fibers oriented in the longitudinal direction [23–25]. The bond behavior between FRP and concrete was extremely hard and complicated because of their complex debonding failure mechanisms, and the material and geometrical nonlinearities of FRP-strengthened reinforced concrete slabs. Multiple factors affect the bond behavior between FRP and the concrete surface, such as the concrete grade [26], length of bonding, axial stiffness of the FRP plate, FRP/concrete ratio, stiffness, and strength of adhesive material [27–29]. Lu et al. [30] studied bond-slip models for FRP sheets/plates bonded to concrete by using the results of 253 pull tests on simple FRP-to-concrete bonded joints. The results concluded that a more accurate model is required. Some researchers have studied strengthening PT concrete elements using FRP. Mohamedien et al. [31] investigated the behavior of hollow core pre-stressed slabs. Nine slabs with dimensions 5.0 m span, 1.2 m wide, and 0.2 m thickness. The slabs were strengthened using CFRP strips and sheets with various arrangements. It is observed that strengthening slabs using CFRP increased the flexural capacity by 40%. Chakrabarti et al. [32] experimentally investigated unbonded PT slabs using slab specimens repaired with different patterns of CFRP. They concluded that using CFRP in repairing slabs reduced the frequency at the high moment region and the crack width and the repaired PT slabs results showed preferable serviceability conditions. As a result of no de-bonding of CFRP sheets, the flexural capacity of the slabs obviously increased. Mohamed et al. [33] studied the flexural behavior of two-way P.T slabs pre-strengthened with external CFRP laminates. The laboratory testing involved four P.T simply supported concrete slabs. They concluded that when compared to control specimens, the P.T concrete slab with bonded tendons and strengthened with CFRP strips showed improvements in ductility, initial stiffness, and deflection of 62.18%, 58.2%, and 37.8%, respectively.

Due to advancements in computing technology and high-end computers' computational power, more research has been done on the behavior of concrete [34,35]. In the field of PT slab strengthening applications, some researchers studied the effect of different FRP strengthening methods. Mahmood et al. and Abdulamier et al. [36,37] have presented a novel approach to simulate lab-strengthened slabs with CFRP (Carbon-Fiber-Reinforced-Polymers) laminates using ANSYS. It is concluded that the study gave good agreement with the experimental results. El Mesk and Harajli [38] examined the effect of strengthening unbonded post-tension (PT) one-way slabs using FRP laminates. The results indicated that strengthening using FRP sheets increases the flexural stiffness and capacity of slabs without a considerable reduction in ductility. The behavior of PT slabs strengthened with CFRP laminates has been modeled using 3D finite-element (FEM) models.

2. Research Significance

To date, from the literature survey, it is observed that there were no previous works that have studied the performance of two-way PT slabs pre-strengthened with external CFRP either experimentally or analytically except, lately, the experimental work of [33]. The purpose of the early use of CFRP strips in slab fabrication was to identify the corresponding stiffness and capacity of PT concrete slabs having such combinations of bending resistance systems. Therefore, in this paper, the response of two-way post-tensioned reinforced concrete (RC) slabs pre-strengthened with CFRP strips is investigated by carrying out a numerical study using ANSYS software to evaluate the significance and sensitivity of the structural responses. The parameters considered in this investigation were the pre-compression ratio, bonded and unbonded tendons, ductility index, and real load simulations besides the effect of ratio and locations of external CFRP strips on the overall slab capacities.

3. Experimental Procedure

Experiments were performed by [33], on five half-scale simply supported PT slabs with overall length, width, and depth of 2370, 2370, and 150 mm, respectively, and the slabs were supported with a clear span of 1800 mm on each side, as shown Figure 1a. Both bonded and un-bonded post-tensioned techniques were used in specimens. On the other hand, 1 MPa and 2 MPa were used as the pre-compression ratio in specimens, number of tendons in X-direction and number of tendons in Y-direction. Each specimen was reinforced with four 10 mm steel bars in addition to the pre-stressing steel because this was the minimum amount of bonded reinforcement needed above columns in both the X and Y directions, as shown in Figure 1a. As shown in Table 1, four slabs (UN, US, BN, and BS1) had the same prestressing tendon layout, as shown Figure 1b,c of the unbonded sample UN, US, and the bonded sample BN, BS1, respectively. One had another tendon layout (BS2), which was double the number of tendons, as shown Figure 1d. Two of the tested slabs were tested without strengthening, as shown Figure 1e, as control slabs (one was bonded, BN, and the other was unbonded; UN), whereas the other three were strengthened using CFRP laminates using the same strengthening scheme (two were bonded, BS1 and BS2, and the other one was unbounded, US). According to [33] tendon handling, unbending was done by means of using coating with corrosion-inhibiting grease and encasing in plastic sheathing. On the other hand, the bonded tendons were placed inside a duct that was injected with cementitious grout after applying prestressing. In addition, the slab samples were designed as per international standards [39–43]. The concrete mix was intended to have a cube compressive strength of 40 MPa. The mix contains 1024 kg/m^3 coarse aggregates with a nominal maximum size of 12.5 mm, and 447 kg/m^3 fine aggregates. Overall, 560 kg/m^3 CEM I 42.5N Portland cement was used. Sika® ViscoCrete® 5930, Sika company, Egypt, is a third-generation super plasticizer for concrete that was added to the mix to ensure workability. One hour before casting, concrete was patched from a ready-mix concrete plant. The same concrete mix was used to cast all the specimens. The cylinders were tested at the same time of testing the specimen in compression and tensile strength. The test-setup of specimens were mounted symmetrically relative to the center of the span with four concentrated point loads and separated by a distance equal to 1/6 of the span length to simulate as accurately as possible the moment diagram generated using the uniformly applied load, as seen in Figure 2. The load was applied statically at a rate of approximately 2 kN/min. All the data was obtained via a framework for data processing. Both strain gauge, LVDT and load cell data were processed within a PC computer and subsequently exported to Excel spreadsheet for analysis. Figure 3 and Table 2 show the load-deflection curves of all tested slabs and all other recorded results [33].

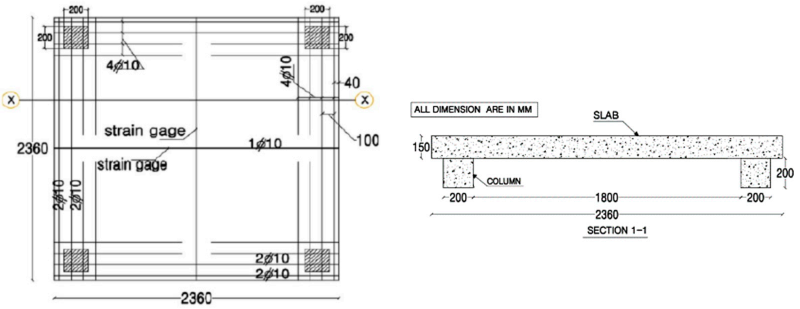

(**a**) Specimen dimensions and reinforcement.

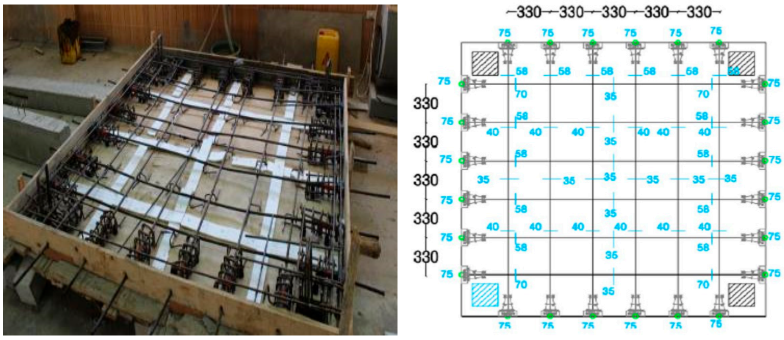

(**b**) UN-bonded tendon slab with 1 MPa, of the sample UN and US.

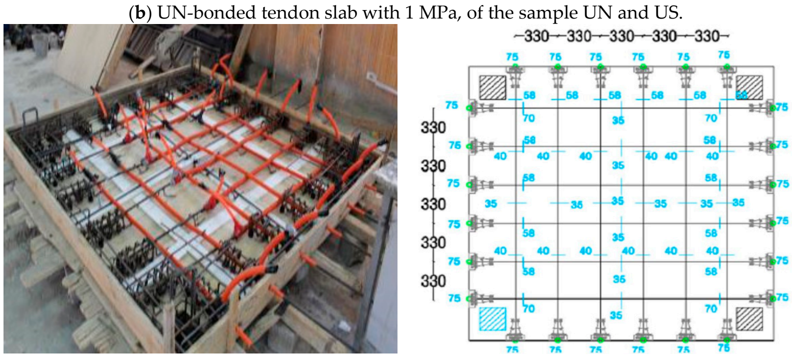

(**c**) Bonded tendon slab with 1 MPa, of the sample BN and BS1.

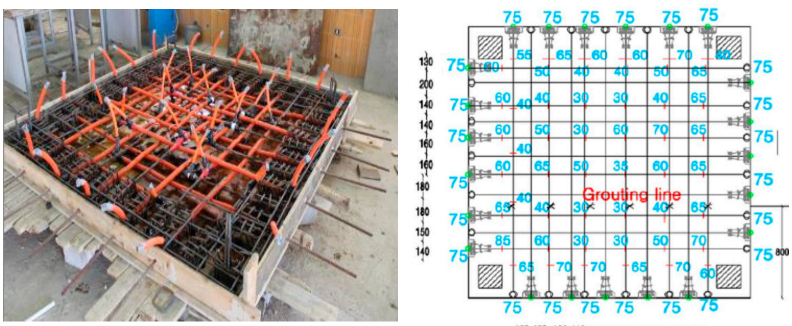

(**d**) Bonded tendon slab with 2 MPa, of the sample BS2.

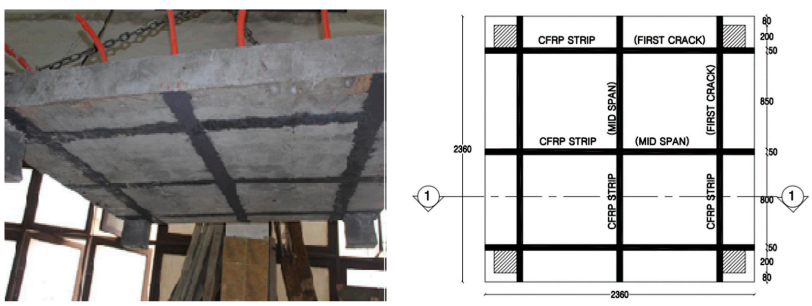

(**e**) Slabs strengthen with CFRP strips.

Figure 1. Typical details for all slabs [33].

Table 1. Summary of specimen's type.

ID	Specimen Types	Test Parameters	
		Type of Prestressing	Pre-Compression Ratio in (X- and Y-Direction)
UN	Unbonded Control Slab	Unbonded	1 MPa
US	Unbonded Slab with CFRP Laminate	Unbonded	1 MPa
BN	Bonded Control Slab	Bonded	1 MPa
BS1	Bonded Slab with CFRP Laminates	Bonded	1 MPa
BS2	Bonded Slab with CFRP Laminates	Bonded	2 MPa

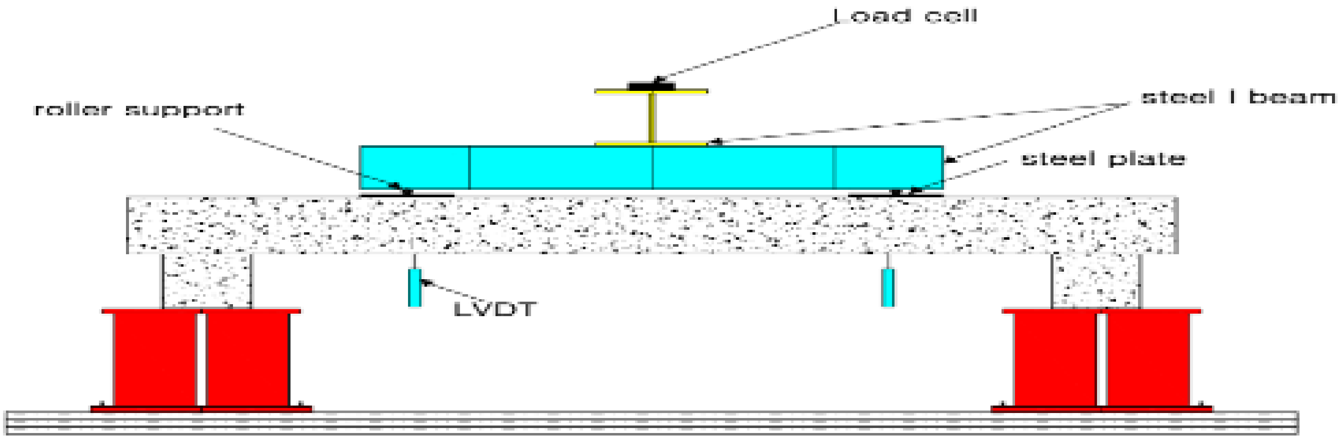

Figure 2. Test setup and instrumentation of slabs specimens [33].

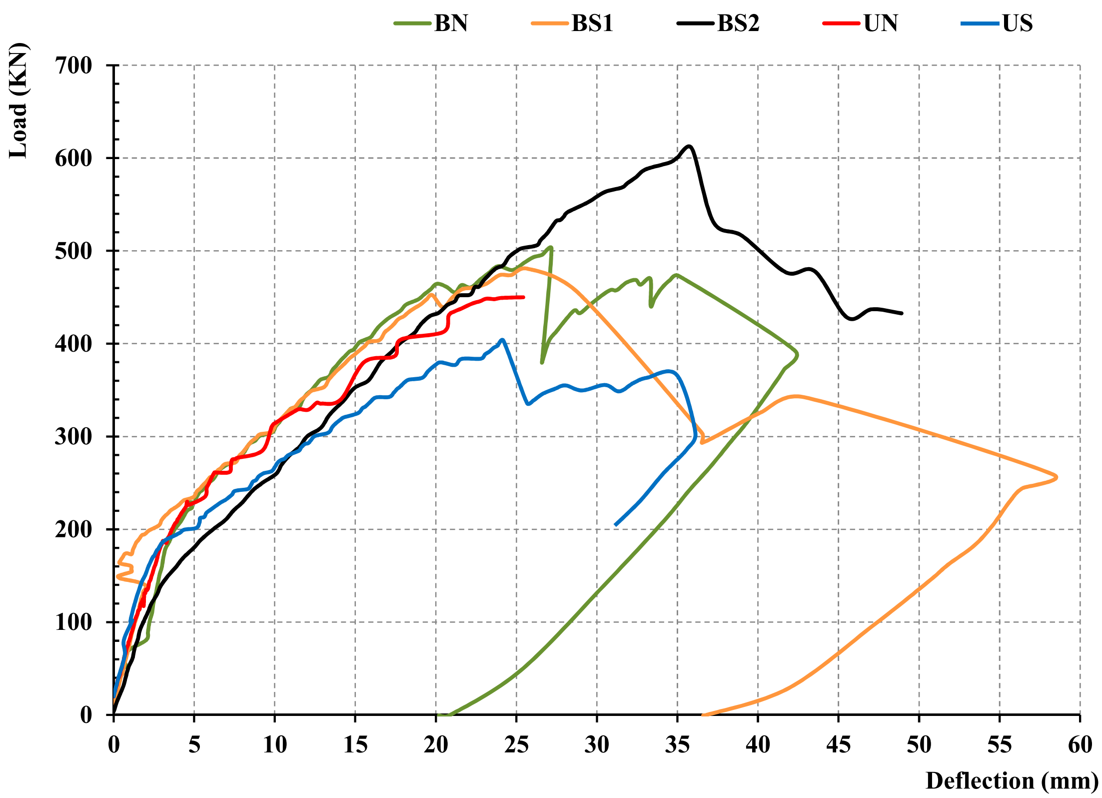

Figure 3. Load-deflection curve of all tested slabs [33].

Table 2. Cracking, ultimate loads and deflections for tested slabs.

ID	Pcr KN	Δcr mm	Pu KN	Δu mm	Δmax mm	Strain CFRP (%)	K Initial	K Post Cracking	Ductility Index
UN	177	1.4	450	11	17	—	66	14	2.2
US	151	1.71	403	24.3	46.8	38%	88	11.2	3.6
BN	179	3.2	502	27	44	—	56	13	2.8
BS1	150	11	480	25	58	34%	88	12	5.3
BS2	169	4.31	610	35.8	48.9	40%	51.2	21.1	8.1

4. ANSYS Finite Element Model

The FEM models were developed using ANSYS-version 15.0 [44]. To save computational time, only one-quarter of each slab was modeled. Direct mesh generation was used to control the model completely; however, it consumed considerably more time than the solid modeling technique. The behaviors of concrete, steel reinforcement, CFRP, and epoxy adhesive were modeled using appropriate element types and constituent models for materials, which were carefully modeled to simulate the experimental trend [33].

4.1. Main Elements Material and Modeling

A. Concrete

The failure of concrete was defined by a multi-linear stress–strain response along with the William and Warnke model [45]. Under uniaxial compression, the behavior of concrete was non-linear plastic obtained from the model of Hognestad [46], as presented in the following equations and shown in Figure 4a,b.

$$f_c = f'_c\left[\left(\frac{2\varepsilon_c}{\varepsilon_0}\right) - \left(\frac{\varepsilon_c}{\varepsilon_0}\right)^2\right] \qquad for\ 0 \le \varepsilon_c \le \varepsilon_0 \tag{1}$$

$$f_c = f'_c - \frac{0.15\, f'_c}{(\varepsilon_{cu} - \varepsilon_{c0})} \qquad for\ \varepsilon_0 \le \varepsilon_c \le \varepsilon_{cu}, \qquad \varepsilon_0 = \frac{2fc}{E_c} \tag{2}$$

where *fc* is the compressive stress at any strain *εc*, *f′c* and ε_0 are the maximum compressive stress and its corresponding strain, *εcu* and fu are the ultimate strain and its corresponding stress which are assumed to be 0.003 and 0.85f′c, respectively; and *Ec* is the initial concrete Young's modulus taken as $4700\sqrt{f'_c}$ [47,48].

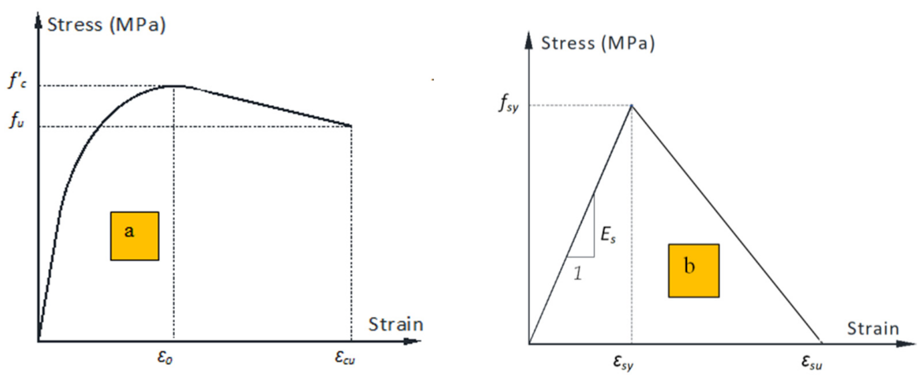

Figure 4. Concrete constitutive models for (**a**) compression and (**b**) tension.

Figure 4b shows the curve of concrete tensile stress–strain. In ANSYS, release 14.0 Documentation, 2015 [48], tension softening is the ability of cracked concrete to pick up tensile stresses between cracks. The rapture strength f_t of concrete was adopted as $0.62\sqrt{f'_c}$, whereas the open and closed shear crack coefficients were set to 0.20. From ANSYS Elements, SOLID65 was used to model concrete due to its capability to produce concrete crushing as well as tension rupture [44,47,48].

B. Steel Reinforcement and Plates

Figure 5 shows the behavior of the steel reinforcement that has an elastic-perfectly plastic non-linear response with a Poisson's ratio of 0.30. The yielding phenomenon defined by the von Mises criterion was employed to define steel performance that was assumed to have a linear elastic material with E and μ of 183 GPa and 0.30, respectively. From ANSYS elements, LINK180 is used to model steel reinforcement [49]. The loading and supporting apparatus were modeled using the eight-node solid brick element SOLID185. This element has eight nodes with three degrees of freedom at each node, displacements in the global x, y, and z directions, and among its characteristic's plasticity, stress stiffening, and large deformations, as well as nonlinear properties such as multi-linear modeling. Precautions were taken to the nearby concrete to prevent impulsive local failure due to stress concentration under loading plates. Besides, the crushing capability of nearby concrete elements, SOLID 65, was removed [50].

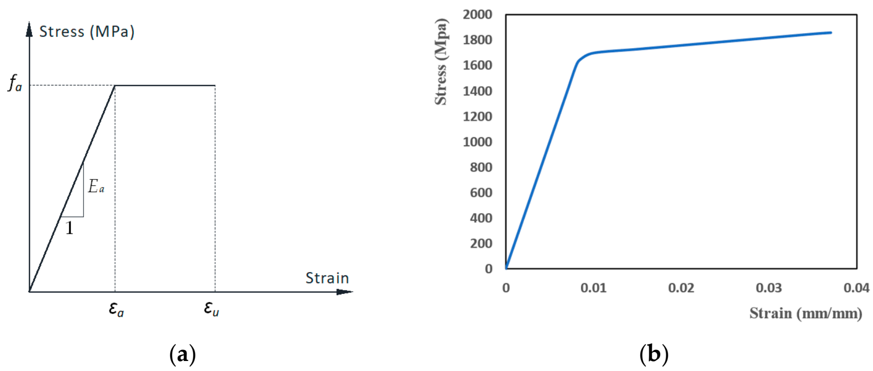

Figure 5. (**a**) Steel constitutive material model, (**b**) stress strain curve of cables.

C. CFRP Laminates and Epoxy Layers

The CFRP laminate material was considered linear elastic isotropic with a Poisson's ratio of 0.35. The behavior of the epoxy adhesive layer with the identical concrete cracking model was defined by a multi-linear elastoplastic diagram without considering the phenomenon of tension softening. The Poisson's ratio was taken as 0.37 for the epoxy adhesive. The schematic stress–strain curves assigned to the two materials are shown in Figures 6 and 7 [49]. SOLID185 layered elements that represent in-plane layered thick shells were used for modeling both CFRP laminates and adhesive epoxy layers. It must be noted that the in-plane stiffness in such elements is the average of all individual layer stiffnesses [48,49].

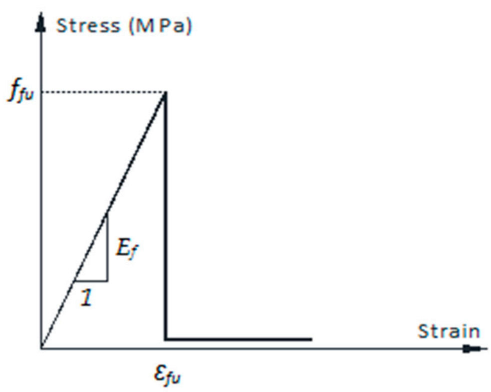

Figure 6. Stress–strain curves for CFRP laminate.

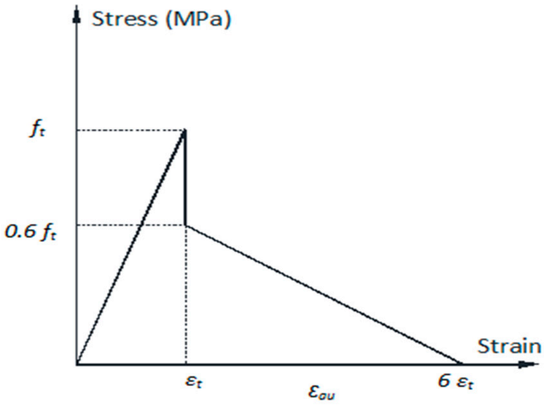

Figure 7. Stress–strain curves for epoxy adhesive.

D. Epoxy/Concrete and Epoxy/CFRP Interfaces

A continuum damage approach (CDM) was used to analyze epoxy–concrete interface debonding with one of the fracture mechanics modules. Delamination or fracture along an interface between different layers plays a basic role in limiting the ductility and the toughness of the multi-phase materials, such as laminated composite structure. This has motivated much research on the failure of the interfaces in which modeling was done by traditional fracture mechanics methods such as the nodal release technique [51,52]. Additionally, the so-called cohesive zone material (CZM) technique, that is used in the current work, is aimed to directly introduce fracture mechanisms by adopting softening relationships between tractions and the separations, which in turn introduce a critical fracture energy that is also the energy required to break apart the interface surfaces. CZM modeling was implemented as given in Ref. [47], in which the discontinuity is technically avoided in Ansys analysis. The CZM model consists of a constitutive relation between the traction T acting on the interface and the corresponding interfacial separation δ (displacement jump across the interface). In ANSYS, the modeling of the CZM traction–separation can be simulated by considering contact elements with zero thickness and interface elements with finite thickness, such as touch components CONTA173, and TARGE170 and interface component INTER205, as given in Figures 8 and 9, respectively [47].

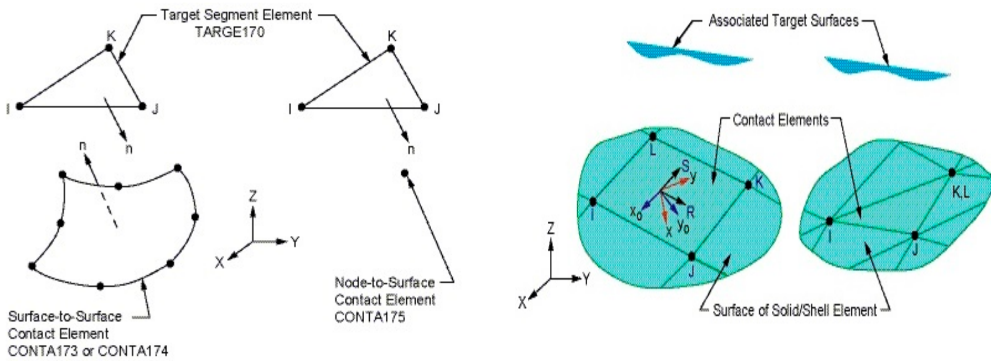

(**a**) Geometry of CONTA173 (**b**) Geometry of TARGE170

Figure 8. The geometry of interfacial contact pair elements.

E. CFRP Slippage

The bond–slip relationship adopted by [50] was used to simulate FRP–concrete interfacial behavior. Figure 10 shows the relationships that comprised interfacial stress (shear) and related gliding slip between the FRP laminates and concrete faces [48,50].

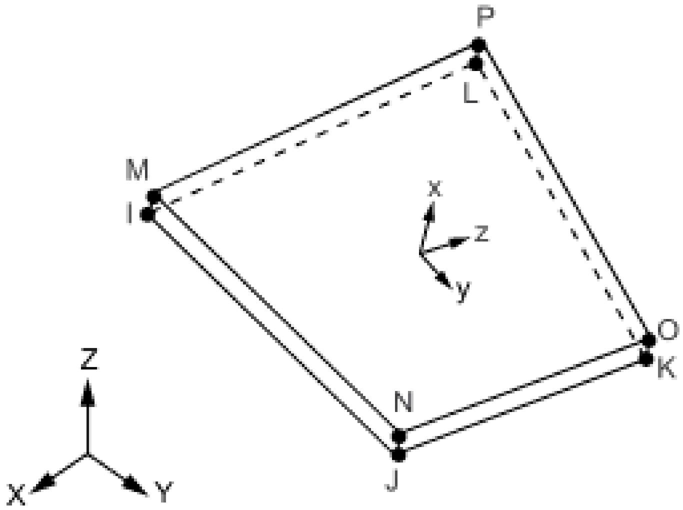

Figure 9. Geometry of INTER205 interface element.

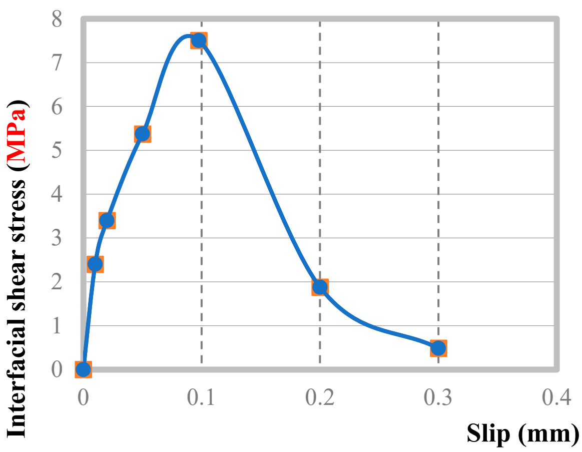

Figure 10. Relationships between the local shear stress and the associated slip.

F. Bonded and Unbonded Cable Modeling

LINK180 was used to model the unbonded cables of PT slabs. PT force is transferred to concrete by end anchorages, in which cables are linked to the slab at the end of anchorages. To prevent stress-concentration, steel plates were added at the location of loading. A similar approach was used to prevent local concrete failure as done here for portions of applied concentrated loads (refer to Section B; Steel Reinforcement and Plates).

Simulation of the bonded tendon through the ANSYS program elements library was like the interface system discussed before in contact surfaces for CFRP laminates and epoxy layers. Again, the contact pair manager method was selected to model the contact between the concrete and the tendon [37]. Application terms of this method are defining two surfaces: one of them is the target and the other is the contact surface. The part of the concrete face contact cable is considered a rigid face and is modeled as the target face within this model (TARGE170). A contact, sliding, and the deformable surface is defined as the tendon surface, which is modeled by the contact surface (CONTA175). In this system, a zero-friction assumption was selected to model contact between the concrete surfaces and unbonded prestressing tendons. The model could not allow the unbonded tendons and concrete surfaces to penetrate each other, although each of them could displace compared to the other. Furthermore, the unbonded prestressing tendon retains its profile during deformation in both transversal and lateral directions (i.e., y- and z-directions, respectively) to ensure compatibility [50].

4.2. FEM Meshing

Figure 11 shows the mesh discretization used in the developed models for all types of slabs. Very fine mesh sizes were selected (12.5 mm) for the whole half-scale model [36,48].

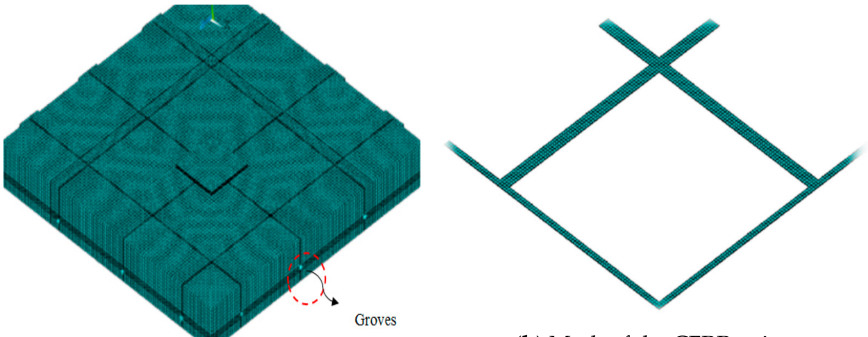

(**a**) Mesh of the developed FEM (**b**) Mesh of the CFRP strips

Figure 11. FEM half-scale model meshing.

4.3. Loading and Boundary Conditions

For symmetry, only half-sized slabs were modeled in which symmetrical constraints were applied at the boundaries of cut lines. Models were limited to simulating experimental works for only one-bay slabs. The four-point loading was applied, as seen in Figure 12. The FEM models were loaded exactly at the same positions located in the experimental work of [33], in which the loading and support patch dimensions were 200 mm × 200 mm × 12.5 mm and 200 mm × 200 mm × 350 mm, respectively. A 12.5 mm thick steel plate was added at the support location to prevent stress-concentrating issues. As stated earlier, Solid185 elements were used to model it, which offered a more balanced distribution of tension over the support field. Moreover, to facilitate the rotation of the slab, a single-line support was mounted under the centerline of the steel plates [53–56].

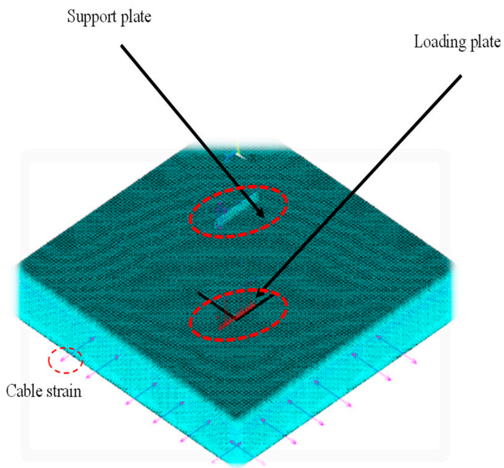

Figure 12. Loading and support locations.

4.4. Stepped Analysis

A force-displacement control method is utilized for solving non-linear analysis associated with a gradual load increase of 1 kN load increment up to failure. Due to the complexity of the solution that consumes much time and due to the non-linear behavior of all elements, it was difficult to achieve solution convergence for the developed models. Therefore, the force convergence tolerance limit was increased from 0.005 (the default tolerance limit defined in ANSYS) to 0.10 for shortening run-time without any loss in solution accuracy. The Newton–Raphson equilibrium iterations were used to update the global stiffness matrix after the completion of each load increment.

4.5. Model Calibration and Validation

Numerical results obtained using FEM analysis for the two unbounded and three bonded slab specimens were compared with the test results produced in the experimental work of [33], for validation. To compare the model conditions with the test setup, a design strip was selected for the critical sagging and hogging areas of the slab in which the lines of zero shear in the x-direction (i.e., about the y -axis) are located. The design strip width was bounded at the column center line as shown in Figure 13, and the following initial values were input.

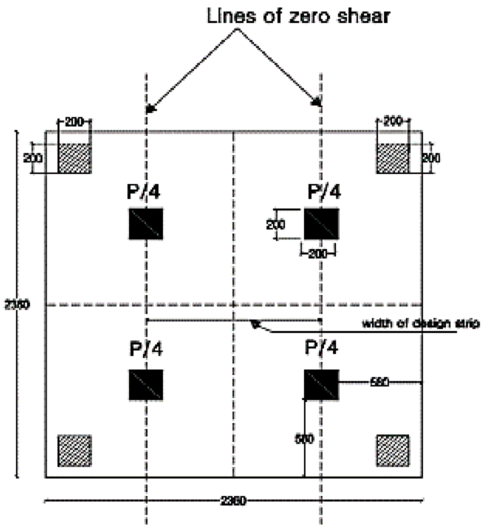

Figure 13. Design strip for model calibration.

(A) Comparison of Camber

Camber deflection due to prestressing force is calculated by the load balancing method as follows:

$$\Delta = \frac{PeL^{\,3}}{8\,EI} \tag{3}$$

where:

P: prestressing force,
E: modulus of concrete,
e: eccentricity of cable from centerline,
I: a gross moment of inertia,
L: length of the slab.

A comparison between the cambers obtained from the test with the others obtained from the model is given in Table 3, which provides an acceptable margin.

Table 3. Values comparison of Δcamber.

Δ Camber (Test)	Δ Camber (ANSYS)
0.859 mm	0.742 mm

(B) Applying of Initial Strain of Tendons

In ANSYS, there is no direct method to impose initial strain on the link element (tendons). To overcome this, initial pre-strains were applied only at the first load step that simulates the measured values given in [33]. Considering the compatibility between concrete and carrying tendons, the application of initial strains was imposed directly on concrete.

4.6. First Crack Monitoring

According to the experimental loading rate listed in Ref. [33], continuous measuring of loads, deflections, and crack monitoring were recorded during all test stages. The first flexural crack was observed visually at a certain load value then it was later verified from the recorded load-deflection curves at the point at which a remarkable change in the slope at nearly the same load level has occurred.

5. Results and Discussion

5.1. Load Deflection Behavior

Figures 14–18 show the FEM deflection contour and Figures 19–23 compare the numerical and experimental (P–Δ) curves for the five slabs. Good agreement was obtained between the FEM model and experimentally obtained results [33]. Table 4 and Figures 24–26 present the comparison details concerning the ultimate load, cracking load, and its corresponding deflection. The ratio between the experimental and FEM results of the first cracking load varied from 0.7 to 0.9, whereas the results of the ultimate load varied from 0.8 to 1.1 and the ultimate deflections varied from 0.8 to 1. It has to be noted that the cause of results ratio differences would be the differences between the experimental environment and modeling. On the other hand, the strain in the CFRP laminates varied between a minimum of 34% and a maximum of 38% of the specified manufactured rupture strain. Generally, it is ensured numerically that the use of CFRP strengthening laminates has significantly increased the ductility index of both bonded and unbonded PT concrete slabs by 62.18% and 59.87%, respectively.

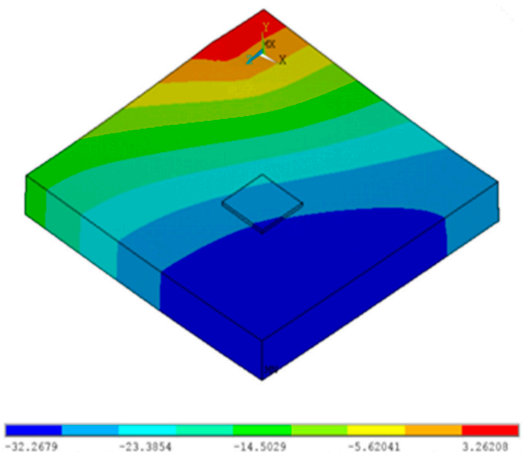

Figure 14. Deformation shape of BN slab.

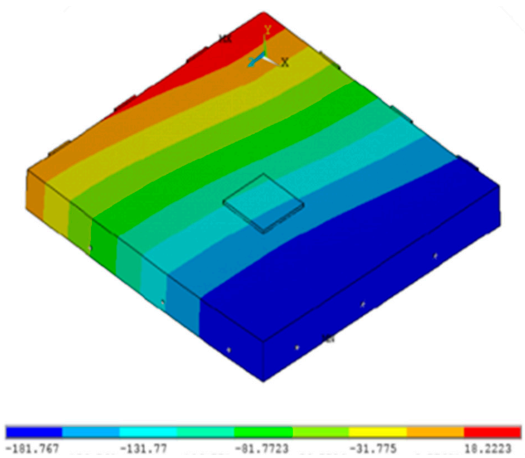

Figure 15. Deformation shape of UN slab.

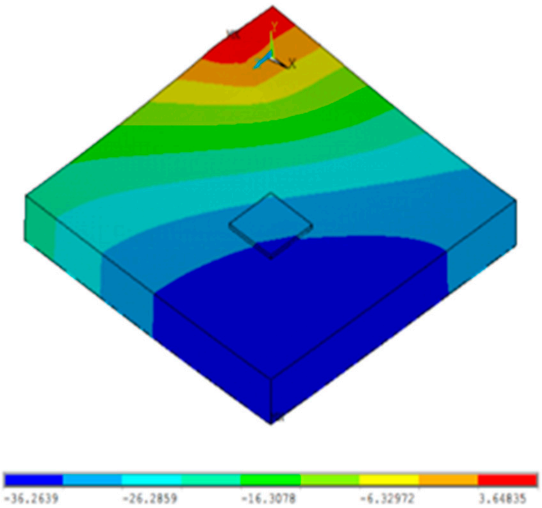

Figure 16. Deformation shape of BS1 slab.

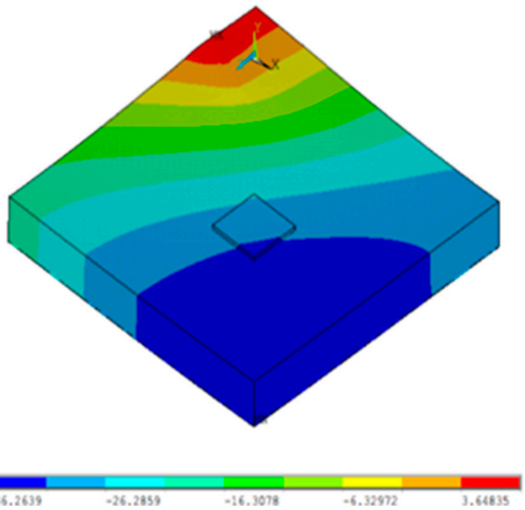

Figure 17. Deformation shape of BS2 slab.

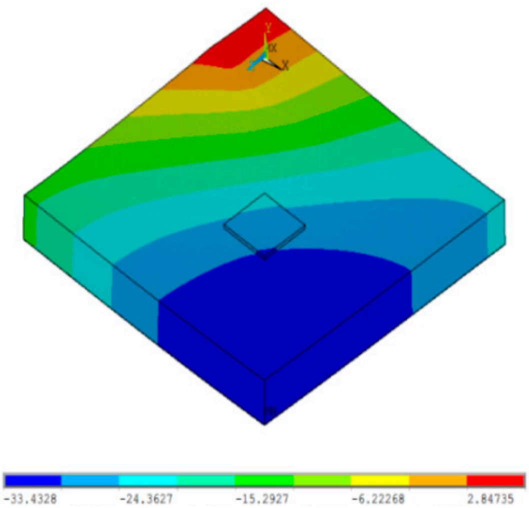

Figure 18. Deformation shape of US slab.

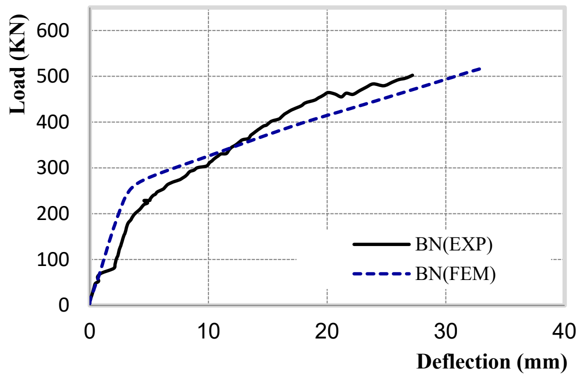

Figure 19. Load-deflection curve of BN slab.

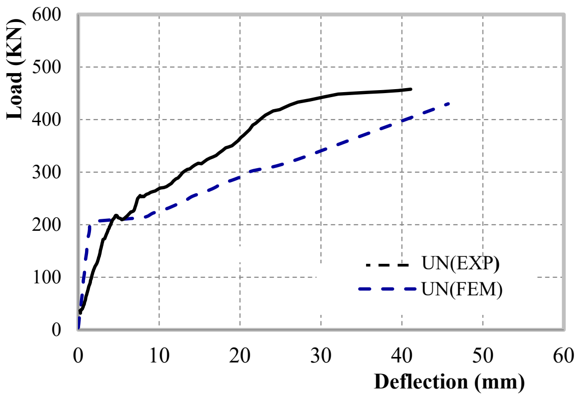

Figure 20. Load-deflection curve of UN slab.

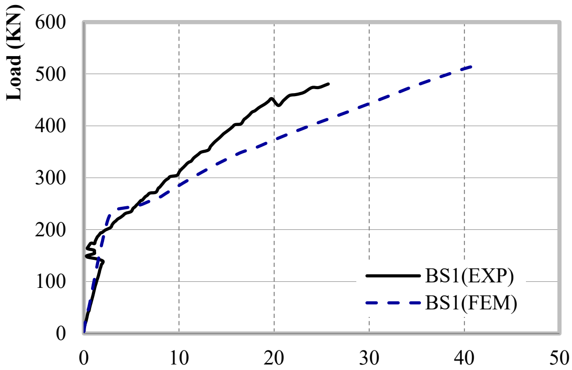

Figure 21. Load-deflection curve of BS1 slab.

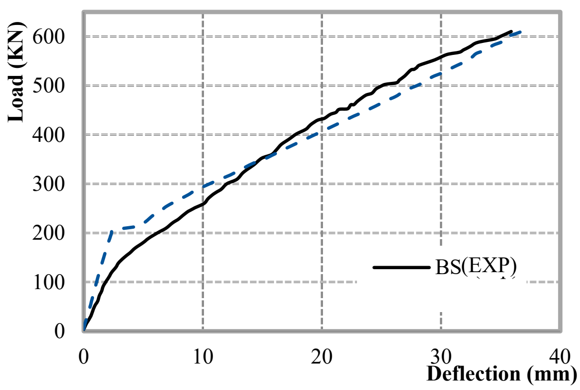

Figure 22. Load-deflection curve of BS2 slab.

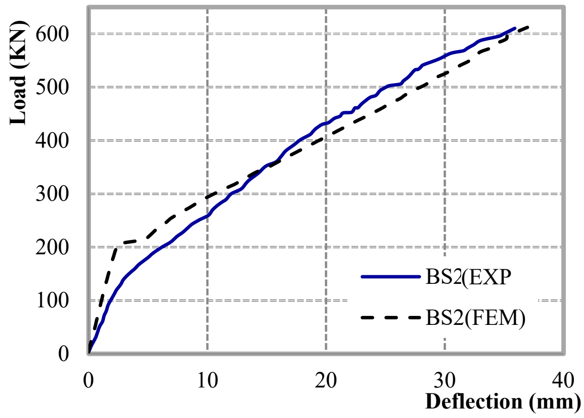

Figure 23. Load-deflection curve of US slab.

Table 4. Experimental and FEM of cracking load, ultimate load, and ultimate deflection.

Slab ID	Cracking Load (KN)			Ultimate Load (KN)			Ultimate Deflection (mm)		
	EXP	FEM	EXP/FEM	EXP	FEM	EXP/FEM	EXP	FEM	EXP/FEM
UN	177.4	200	0.9	450	420	1.1	40	45	0.9
US	150.63	210	0.7	403.3	500	0.8	24.3	30	0.8
BN	179.4	250	0.7	502	520	1	27	33	0.8
BS1	149.6	220	0.7	480	500	1.1	25	29	0.9
BS2	150	200	0.8	600	605	1	35	36	1

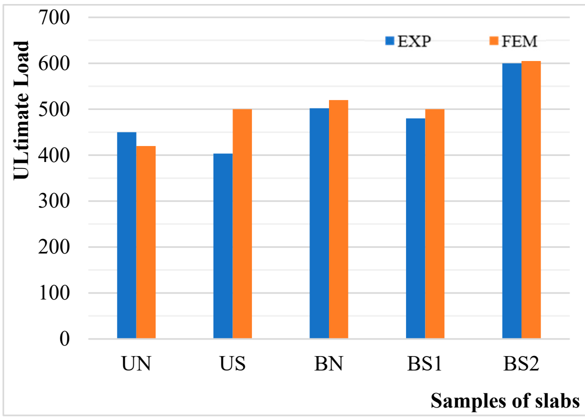

Figure 24. Ultimate load comparison between FEM and EXP.

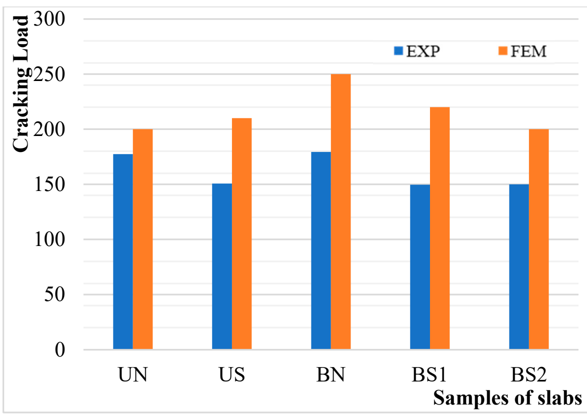

Figure 25. Cracking load comparison between FEM and EXP.

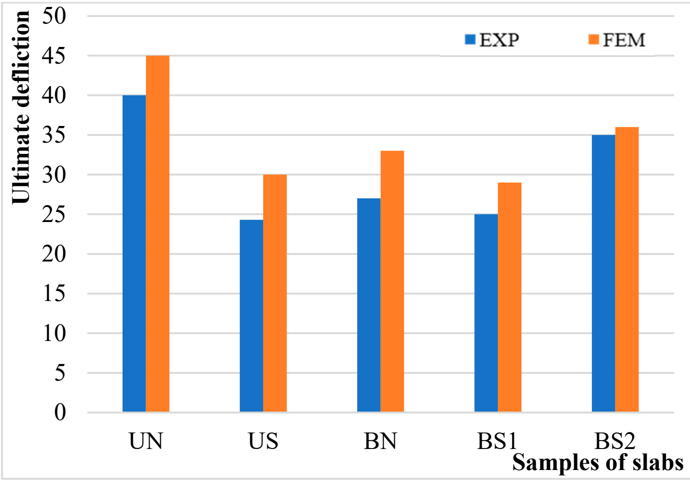

Figure 26. Ultimate deflection comparison between FEM and EXP.

Further analysis reveals that the achieved ultimate loads from experimental results, EXP, are somewhat less than those obtained from FEM models. This is because of ignorance of the radial stresses exerted by the tendon on the concrete cover in the developed FEM models. The FEM-EXP difference between the cracking loads and ultimate deflections lies within the usual tolerance and could be attributed to the modeling deviations from real situations. Regarding deflection behavior, Figures 19–23 show that the FEM models of slabs had nearly the same trend as the tested specimens except at the end parts; this remark can be attributed to the technical problem that had occurred during the slab test in the laboratory that caused the test to be stopped [33]. However, the differences of pre-yield stiffness are in the accepted range.

5.2. Concrete and CFRP Strain Behavior

At different loading levels, there is a good correlation between FEM results and experimental concrete and CFRP strains. Figures 27 and 28 clearly illustrate this match for two types of slabs, whereas Figure 29 demonstrates the final debonding stage of CFRP for BN slab in which the locations of slippage matched exactly the experimental observations.

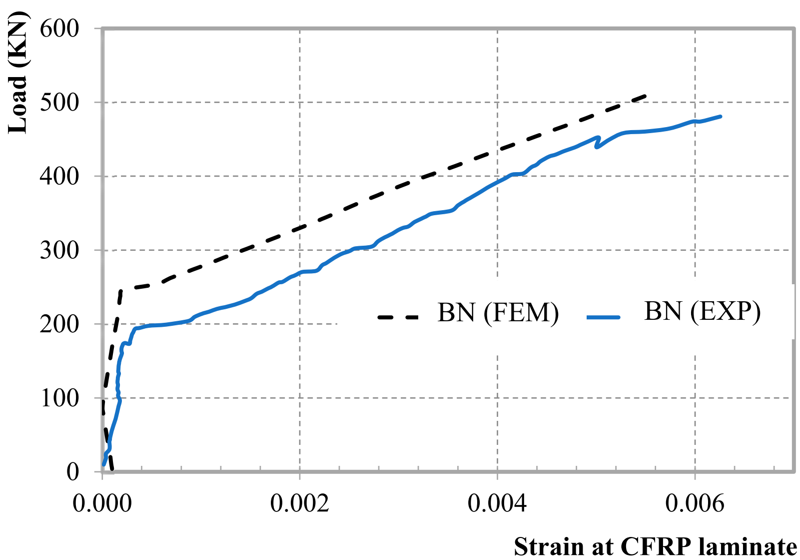

Figure 27. General comparison between EXP and FEM for CFRP strain for BN slab.

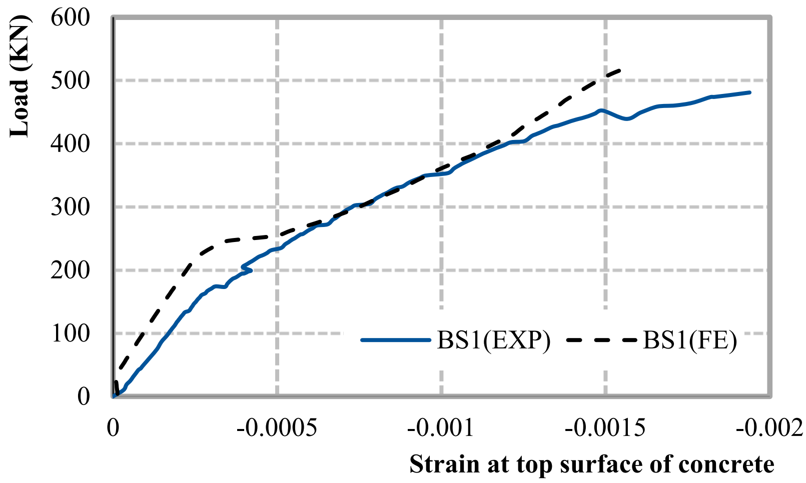

Figure 28. Comparison between EXP and FEM for the concrete strain of BS1 slab.

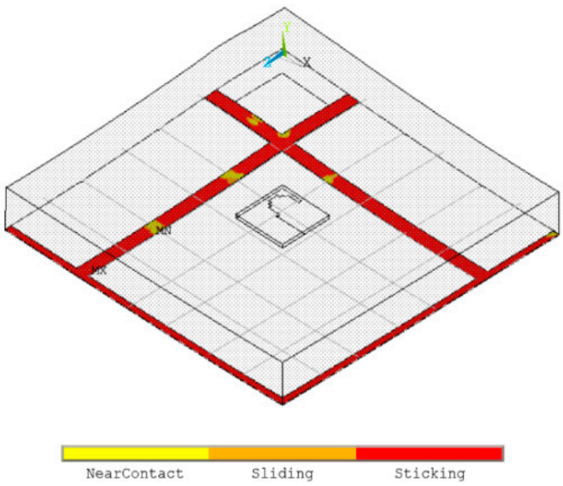

Figure 29. Final stage of CFRP laminates debonding in BN slab model.

5.3. Failure Modes

The failure stage of tested slabs can be expected to be either of the following:

a. Concrete crushing; when the strain of concrete reaches 0.002,
b. Tendon cut; due to reaching its ultimate capacity (not occurring here),
c. CFRP debonding; concrete cover or CFRP laminate separation at the surface plane.

The energy criteria or the stress-intensity-factor criterion are usually used in fracture analysis. The critical value of the magnitude of the stress and deformation fields characterizes the fracture toughness when the stress-intensity-factor criterion is applied. The von Mises failure criterion and the William and Warnke model are used by the multilinear isotropic material to define concrete failure. The research done by Kachlakev et al. [47] served as a foundation for calculating the shear transfer coefficients for open and closed cracks. When the shear transfer coefficient for the open crack fell below 0.2 and the coefficient for the open and close cracks were both set to 0.2, convergence issues appeared. The modulus of rupture was used as the basis for the uniaxial cracking stress. In this approach, the uniaxial crushing stress was derived from the uniaxial compressive strength. As recommended by earlier studies [47], it was entered as -1 to disable the concrete element's capacity for crushing. When the crushing capability was activated, convergence issues kept occurring.

Basically, the ANSYS program records concrete cracks and crushing at each applied load step. A circle outline in the plane of the crack represents cracking. When the Solid65 element achieves the ultimate strain of 0.002, according to the stress–strain curve of compressed concrete, a crushing limit is immediately applied at that element. An octahedron outline represents crushing. Each integration point can crack into up to three different planes. The first, second, and third cracks at an integration point are shown with a red circle outline, green circle outline, and blue circle outline, respectively, as shown in Figure 30 for bonded and unbonded slab failure development. It was observed that failure modes match exactly what has occurred in experiments [33]. Finally, it is observed that the rigidities of concrete slabs after cracking in the finite element analysis are much lower than those of the test.

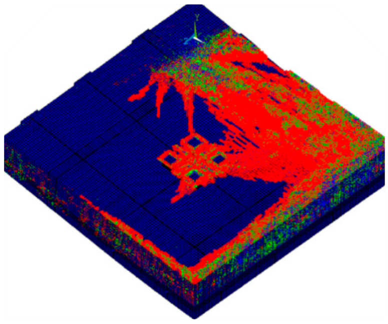

(**a**) Unbonded

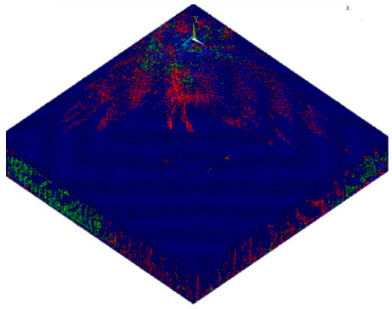

(**b**) Bonded

Figure 30. Progression of cracks.

6. Parametric Study

As the FEM simulation closely matches the experimental results, the developed analytical model was used to examine the effect of changing some main parameters on the flexural performance of bonded PT slabs strengthened with CFRP laminates. Three parameters were studied: real loading simulation schemes, using different arrangements of CFRP laminates, and PT/CFRP strength contribution.

6.1. Real Load Simulation

All tested slabs in [33] were equipped with four equivalent concentrated point loads applied symmetrically relative to the center of the span and separated by a distance equal to 1/6 of the span length to simulate the actual distributed load in real cases. Similarly, the corresponding FEM models were given the same conditions of loading. To represent the effect of real load simulation as a uniformly distributed load, the equivalent values of concentrated loads are put directly as uniform loads. Figure 31 displays the simulation of the real delivery load; meanwhile, Figure 32 shows the comparison between both cases' results, which reflect the sensitivity of this simulation.

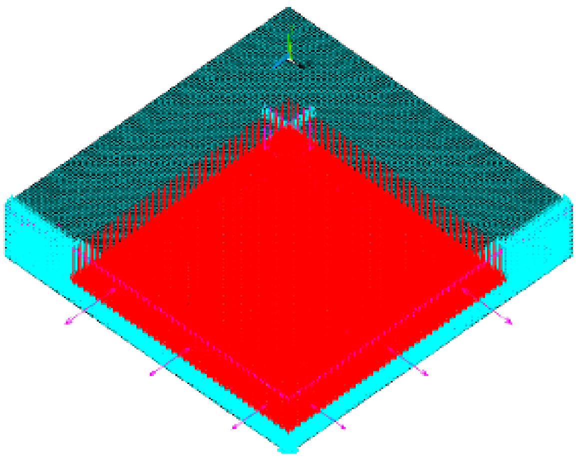

Figure 31. Modeling of uniform load.

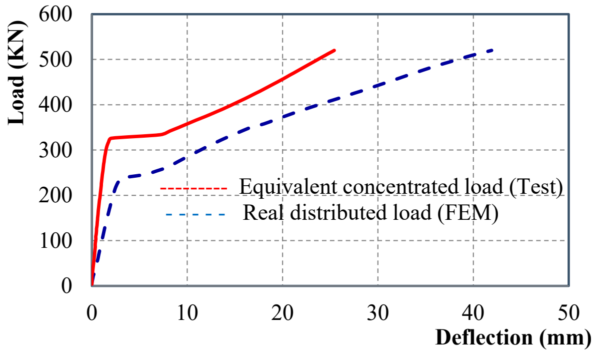

Figure 32. FEM simulation comparison between equivalent test loads and real uniformly distributed load for slab BS1.

6.2. Different Arrangements of CFRP Laminates

To investigate the effect of the optimum CFRP laminate position selection, two different schemes of distribution were investigated. The first scheme of laminate attachment location was selected to be adjacent to columns only (column laminate), and the other was at the middle span only (field laminate), as shown in Figures 33 and 34. From the results, it was observed that the column laminate had a significant impact, such as delaying the first crack load and producing less deflection, as can be seen from Figures 35 and 36.

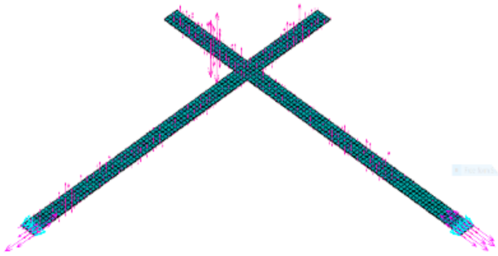

Figure 33. Modeling of CFRP laminate adjacent to columns (column laminate).

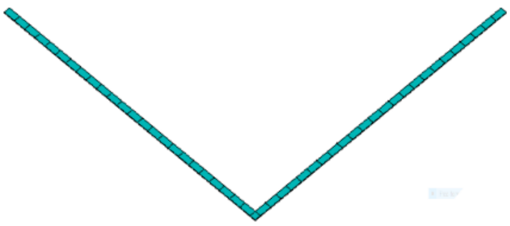

Figure 34. Modeling of CFRP laminate at middle span (field laminate).

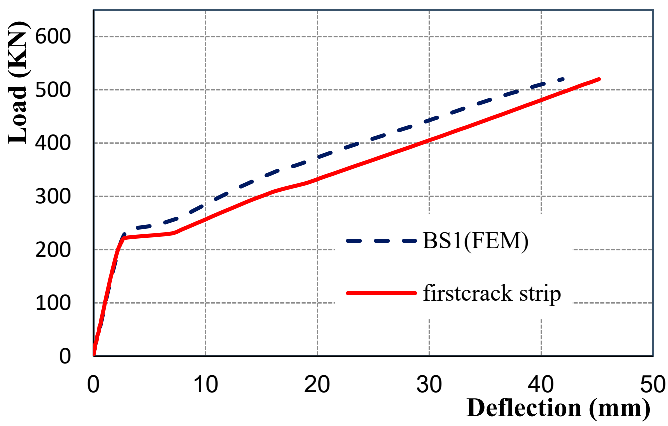

Figure 35. Comparison between column laminate results with BS1.

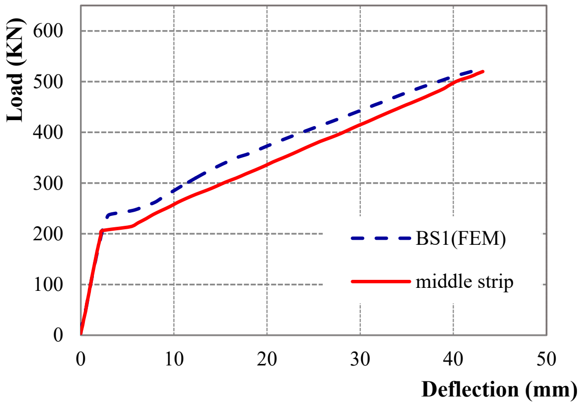

Figure 36. Comparison between field laminate results with BS1.

6.3. PT to CFRP Strength Contribution

As shown in Figures 37–39, different ratios of PT cables (tendons) to CFRP laminates were selected to investigate the strength contribution and how efficient is the use of CFRP strengthening in different cases. From the graphs, it is concluded that the strengthening of CFRP laminates is more significant in cases of low PT reinforcement than that in high PT reinforcement.

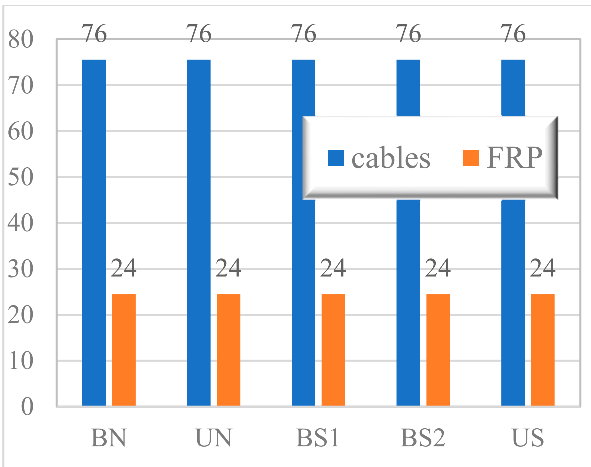

Figure 37. Strength contribution for one cable and one FRP laminate (1:1 ratio).

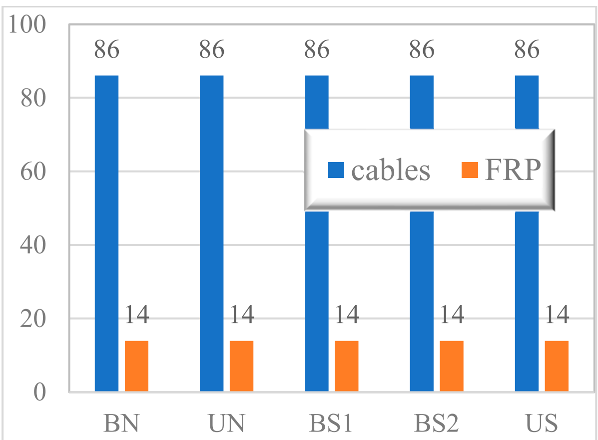

Figure 38. Strength contribution for 6 cables and 3 FRP laminates (2:1 ratio).

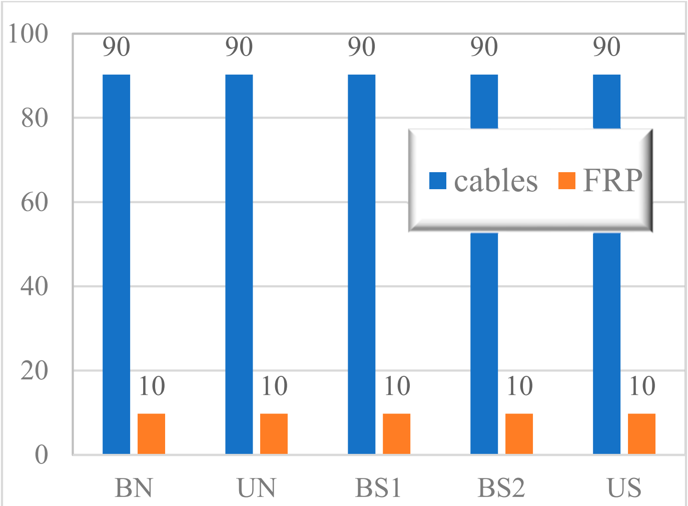

Figure 39. Strength contribution for 12 cables and 4 FRP laminates (3:1 ratio).

7. Conclusions

A hybrid nonlinear finite elements (FEM) model was developed to examine the flexural performance and the ultimate load capacity of bonded and unbonded two-way reinforced concrete post-tensioned (PT) slabs that were pre-strengthened with external carbon-fiber reinforcement polymer (CFRP) laminates. From this study, the following conclusions can be listed:

- The FEM simulation showed great agreement with experimental results. The ratio between the experimental and FEM results of the first cracking load varied from 0.7 to 0.9, whereas the results of the ultimate load varied from 0.8 to 1.1 and the ultimate deflections varied from 0.8 to 1.
- At different loading levels, there is a good correlation between FEM results and experimental results for CFRP strains either for the final debonding stage or for the locations of slippage.
- From both FEM and experiments, it was concluded that the failure modes of the tested slabs were concrete crushing, CFRP rupture, and/or CFRP debonding.
- Performance of the fully prestressed post-tensioned two-way slabs pre-strengthened with CFRP laminates have better performance in bonded rather than unbonded slabs.
- Strengthening using CFRP materials is extremely effective in increasing the ductility index of both bonded and unbonded PT concrete slabs. Ductility increased by 62.18% and 59.87%, respectively, when compared with the control samples.
- Real load simulation rather than test-equivalent criteria is considered a major and sensitive factor that has to be carefully represented in either experimental or numerical simulations to reflect reliable results.
- In selecting an optimized scheme for strengthening PT slabs, it is noted that using laminates adjacent to columns is more efficient than in other slab locations.
- CFRP strength contribution to PT cabling is very considerable in slabs with low PT reinforcement ratios, whereas it is not effective in slabs with larger PT ratios.
- Finally, the results that were obtained using a numerical FEM model with the ANSYS program demonstrated good agreement with experimental results for illustrated slabs.

Further research is recommended to apply CFRP strengthening in existing PT slabs and study the behavior in that case. Additionally, as the slippage or debonding of CFRP laminates was the major outcome in this study, future solutions should be considered to prevent such failure modes to achieve the most efficiency of CFRP strengthening.

Author Contributions: Conceptualization and methodology, M.M.A., A.H.H.K., G.N.M. and M.F.S.; software, validation, formal analysis, data curation, writing original draft preparation, writing review and editing and visualization, M.M.A., G.N.M. and M.F.S.; investigation, M.M.A. and M.F.S.; resources, supervision, and project administration, M.M.A., A.H.H.K., M.F.S. and D.K. All authors have read and agreed to the published version of the manuscript.

Funding: This research received no external funding.

Institutional Review Board Statement: Not applicable.

Informed Consent Statement: Not applicable.

Data Availability Statement: Not applicable.

Acknowledgments: This paper was elaborated with the financial support of the research project VEGA 1/0626/22 of the Scientific Grant agency, the Ministry of Education, Science, Research, and Sport of the Slovak Republic and the Slovak Academy of Sciences.

Conflicts of Interest: The authors declare no conflict of interest.

References

1. Al Mohammedi, A.; Murray, C.D.; Dang, C.N.; Hale, W.M. Practical ultra-high-strength concrete for precast concrete applications. *PCI J.* **2022**, *67*, 29–52. [CrossRef]
2. Mante, D.M.; Isbiliroglu, L.; Hofrichter, A.; Barnes, R.W.; Schindler, A.K. Expected compressive strength in precast, prestressed concrete design: Review and discussion of regional practice. *PCI J.* **2022**, *67*, 53–70. [CrossRef]
3. Bhuiyan, I.H.; Amin, A.; Riyad, R.H.; Sadi, R.; Hasan, M.A. Structural analysis of pre-tensioning and post-tensioning concrete with normal concrete beam. In Proceedings of the International Conference on Planning, Architecture & Civil Engineering, Rajshahi, Bangladesh, 9–11 September 2021.
4. Khalil, A.H.H.; Ashraf, M.; Heniegal, A.; Attia, M.M. Behavior of post-tensioned fibrous lightweight concrete beams made of natural pumice. In Proceedings of the 2nd International Conference, Sustainable Construction and Project Management Sustainable Infrastructure and Transportation for Future Cities, Aswan, Egypt, 16–18 December 2018.
5. Cho, A.S.; Kang TH, K. Computer-based design optimization of post-tensioned anchor for single-strand. *Adv. Comput. Des.* **2021**, *6*, 339–360. [CrossRef]
6. Abdelhalim, J.O.; Sayed-Ahmed, E.Y. Testing post tensioned slabs with bonded and unbonded tendons. In Proceedings of the International Conference on Civil, Structural and Transportation Engineering, Virtual, 17–19 May 2021. [CrossRef]
7. Mirzaee, A.; Ashkan Torabi, A.; Totonchi, A. Experimental study on the behavior of reinforced concrete beam boosted by a post-tensioned concrete. *Comput. Concr.* **2021**, *28*, 549–557. [CrossRef]
8. Fu, C.; Zhu, Y.; Wang, Y. Stiffness assessment of cracked post-tensioned concrete beams with unbonded tendons based on the cracking pattern. *Eng. Struct.* **2020**, *214*, 110599. [CrossRef]
9. Zhou, L.; Mahunon AD, G.; Yin, G.; Xue, X. Experimental investigation of simply-supported post-tensioned beam after anchorage system failure. *Eng. Struct.* **2020**, *212*, 110507. [CrossRef]
10. Elsharkawy HE, A.E.; Elafandy, T.; EL-Ghandour, A.W.; Abdelrahman, A.A. Behavior of post-tensioned fiber concrete beams. *HBRC J.* **2013**, *9*, 216–226. [CrossRef]
11. Zelickman, Y.; Amir, O. Optimization of post-tensioned concrete slabs for minimum cost. *Eng. Struct.* **2022**, *259*, 114132. [CrossRef]
12. Su, M.; Gong, S.; Liu, Y.; Peng, H. Flexural behavior of RC beams strengthened with fully or partially prestressed near-surface mounted FRP strips: An experimental investigation. *Eng. Struct.* **2022**, *262*, 114345. [CrossRef]
13. Piatek, B.; Siwowski, T.; Michalowski, J.; Blazewicz, S. Flexural strengthening of RC beams with prestressed CFRP strips: Development of novel anchor and tensioning system. *J. Compos. Constr.* **2020**, *24*, 04020015. [CrossRef]
14. Triantafillou, T.C. Strengthening of historic structures with advanced composites: A review. In *Recent Advances in Composite Materials*; Softcover reprint of the original 1st ed. 2003 edition; Springer: Berlin/Heidelberg, Germany, 2003; pp. 337–344. [CrossRef]
15. Attia, M.M.; Shawky, S.M. Banana Fiber Reinforced Concrete: A Review. *N. Y. Sci. J.* **2021**, *14*, 48–57.
16. Attia, M.M.; Ahmed, O.; Kobesy, O.; Malek, A.S. Behavior of FRP rods under uniaxial tensile strength with multiple materials as an alternative to steel rebar. *Case Stud. Constr. Mater.* **2022**, *17*, e01241. [CrossRef]
17. Kadhim MM, A.; Altaee, M.J.; Adheem, A.H.; Chabuk, A.; Al-Ansari, N. Review on NSM CFRP strengthened RC concrete beams in shear. *Adv. Civ. Eng.* **2021**, *2021*, 1074010. [CrossRef]
18. Attia, M.M.; Al Sayed, A.A.A.; Tayeh, B.A.; Shawky, S.M.M. Banana agriculture waste as eco-friendly material in fibre-reinforced concrete: An experimental study. *Adv. Concr. Constr.* **2022**, *14*, 355–368. [CrossRef]
19. Rageh, B.O.; El-Mandouh, M.A.; Elmasry, A.H.; Attia, M.M. Flexural behavior of rc beams strengthened with gfrp laminate and retrofitting with novelty of adhesive material. *Buildings* **2022**, *12*, 1444. [CrossRef]
20. Mohammed, M.A.; El-Shaer, M.A.A.; Shawky, S.M.M.; Samaan, M.F. Replacement efficiency of steel reinforcement with FRB bars in RC beams under flexure load: Experimental and FE study. *Innov. Infrastruct. Solut.* **2022**, *7*, 281. [CrossRef]

21. Chansawat, K. Nonlinear Finite Element Analysis of Reinforced Concrete Structures Strengthened with FRP Laminates. Doctoral Thesis, Oregon State University, Corvallis, OR, USA, 2003.
22. Amiri, S.; Behzad Talaeitaba, S. Punching shear strengthening of flat slabs with EBROG and EBRIG—FRP strips. *Structures* **2020**, *26*, 139–155. [CrossRef]
23. Mohamed, T.K.H. Flexural Performance and Bond Characteristics of FRP Strengthening Techniques for Concrete Structures. Doctoral Thesis, The University of Manitoba, Winnipeg, MB, Canada, 2002.
24. Revathy, J.; Sriraman, M. Structural Response of FRP Strengthened Post-Tensioned Concrete Beams. *Res. J. Recent Sci.* **2014**, *3*, 198–202.
25. Siwowski, T.; Piątek, B.; Siwowska, P.; Wiater, A. Development and implementation of CFRP post-tensioning system for bridge strengthening. *Eng. Struct.* **2020**, *207*, 110266. [CrossRef]
26. Gao, D.; Fang, D.; You, P.; Chen, G.; Tang, J. Flexural behavior of reinforced concrete one-way slabs strengthened via external post-tensioned FRP tendons. *Eng. Struct.* **2020**, *216*, 110718. [CrossRef]
27. Jayanna, R.B. Experimental Evaluation of FRP Strengthened Concrete Bridge Girders. Master's Thesis, The University of Texas at Arlington, Arlington, TX, USA, 2015.
28. Chakrabarti, P.R.; Kim, U.; Hong, H.; Busciano, M.; Dao, V. Repair Systems for Post-Tensioned Slabs with Composite Material. *Struct. Eng. Res. Front.* **2007**, 1–13. [CrossRef]
29. Török, I.; Puskás, A.; Virág, J. Post-tensioned Flat Slabs with Unbonded Tendons for Public Buildings. *Procedia Manuf.* **2019**, *32*, 102–109. [CrossRef]
30. Lu, X.; Teng, J.; Ye, L.; Jiang, J. Bond–slip models for FRP sheets/plates bonded to concrete. *Eng. Struct.* **2005**, *27*, 920–937. [CrossRef]
31. Mohamedien, M.A.; Hosny, A.H.; Abdelrahman, A. Use of FRP in Egypt, Research Overview and Applications. *Procedia Eng.* **2013**, *54*, 2–21. [CrossRef]
32. Chakrabarti, P.R.; Kim, U.; Busciano, M.; Dao, V. Repair systems for unbonded post-tensioned 1-way & 2-way slabs with CFRP. In *Challenges, Opportunities and Solutions in Structural Engineering and Construction*; Taylor & Francis Group: London, UK, 2010; ISBN 978-0-415-56809-8.
33. Mohamed, G.N.; Khalil AH, H.; Samaan, M.F.; Hadad, S.H. The flexural behavior of two way post tensioned slabs pre-strengthened with external CFRP laminates. *N. Y. Sci. J.* **2019**, *12*, 14–22.
34. Lee, S.H.; Abolmaali, A.; Shin, K.J.; Lee, H.D. ABAQUS modeling for post-tensioned reinforced concrete beams. *J. Build. Eng.* **2020**, *30*, 101273. [CrossRef]
35. Santarsiero, G.; Masi, A. Analysis of slab action on the seismic behavior of external RC beam-column joints. *J. Build. Eng.* **2020**, *32*, 101608. [CrossRef]
36. Mahmood, M.B.; Agarwal, V.C. Non-Linear Finite Element Analysis of RC Slabs Strengthened with CFRP Laminates. *Int. J. Eng. Trends Technol. (IJETT)* **2013**, *5*, 17403934.
37. Abdulamier, J.; Aziz, A.; Al-Assam, H. Non-linear behavior of unbonded post-tensioned one-way concrete slab panel. *J. Environ. Stud.* **2013**, *10*, 39–45. [CrossRef]
38. El Meski, F.; Harajli, M. Strengthening of unbonded post-tensioned concrete slabs using external FRP composites. In Proceedings of the CICE2012 Conference. 2012. Available online: https://www.semanticscholar.org/paper/Strengthening-of-unbonded-post-tensioned-concrete-%3A-El-Meski/429a896f4a3dcb2cf12fea73c4715f7eb2299a19#citing-papers (accessed on 1 January 2020).
39. *ACI 440.2R-17*. Guide for the Design and Construction of Externally Bonded FRP Systems for Strengthening Concrete Structures. Farmington Hills, MI, USA, 2017. Available online: https://www.concrete.org/store/productdetail.aspx?ItemID=440217&Language=English&Units=US_AND_METRIC (accessed on 1 January 2020).
40. *BS 8110-1*; Part 1: Code of Practice for Design and Construction. 1997. Available online: https://www.thenbs.com/PublicationIndex/documents/details?Pub=BSI&DocID=257098 (accessed on 1 January 2020).
41. *ACI Building Code Requirements for Structural Concrete (ACI 318M-14) and Commentary (ACI318RM-14)*; American Concrete Institute: Farmington Hills, MI, USA, 2021.
42. *ECP203*; Egyptian Code for Design and Implementation of Concrete Structures. 2018.
43. *TR43*; Post Tension Concrete Floors Design Handbook. The Concrete Society: Camberley, Surrey, UK, 2005.
44. ANSYS; Ansys Inc. Documentation. 2015. Available online: http://www.ansys.com (accessed on 1 January 2020).
45. Khalil, A.H.; Heniegal, A.A.; Attia, M.M. Nonlinear finite element analysis of steel fibers reinforced post-tensioned lightweight concrete beam. *N. Y. Sci. J.* **2018**, *11*, 80–92.
46. Barbero, E.J.; Shahbazi, M. Determination of material properties for ANSYS progressive damage analysis of laminated composites. *Compos. Struct.* **2017**, *176*, 768–779. [CrossRef]
47. Kachlakev, D.; Miller, T. *Finite Element Modeling of Reinforced Concrete Structures Strengthened with FRP Laminates*; Oregon Department of Transportation Research Group: Salem, OR, USA, 2001.
48. Abbasi, A.; Benzeguir ZE, A.; Chaallal, O.; El-Saikaly, G. FE Modelling and simulation of the size effect of RC T-beams strengthened in shear with externally bonded FRP fabrics. *J. Compos. Sci.* **2022**, *6*, 116. [CrossRef]
49. Mohammed, A.; Tayşi, N.; Faqe, A.H.; Abdul-Razzaq, K.S. Modelling of bonded post-tensioned concrete cantilever beams under flexural loading. *Civ. Eng. J.* **2017**, *3*, 463–479. [CrossRef]

50. Yu, H.; Bai, Y.L.; Dai, J.G.; Gao, W.Y. Finite element modeling for debonding of FRP-to-concrete interfaces subjected to mixed-mode loading. *Polymers* **2017**, *9*, 438. [CrossRef]
51. Hentati, H.; Naceur, I.B.; Bouzid, W.; Maalej, A. Numerical analysis of damage thermo-mechanical models. *Adv. Appl. Math. Mech.* **2015**, *7*, 625–643. [CrossRef]
52. Materna, A.; Oliva, V. Elastic-plastic FEM investigation of the thickness effect on fatigue crack growth. *Procedia Eng.* **2011**, *10*, 1109–1114. [CrossRef]
53. Teng, X. Nonlinear Finite Element Analysis of FRP-Strengthened Concrete Slabs under Static and Traffic Loads. Doctoral Thesis, University of New South Wales Canberra, Canberra, ACT, Australia, 2013.
54. da Silva, A.R.; de Souza Rosa, J.P. Nonlinear numerical analysis of prestressed concrete beams and slabs. *Eng. Struct.* **2020**, *223*, 111187. [CrossRef]
55. Six, P.; Tawadrous, R.; Syndergaard, P.; Maguire, M. Flexural behavior of three span continuous unbonded post-tensioned members with variable bonded reinforcement. *Eng. Struct.* **2019**, *200*, 109704. [CrossRef]
56. Degtyarev, V.V. Concentrated load distribution in corrugated steel decks: A parametric finite element study. *Eng. Struct.* **2020**, *206*, 110158. [CrossRef]